# Effects of sample disturbance on the stress-induced microfracturing characteristics of brittle rock

**E. Eberhardt, D. Stead, and B. Stimpson**

**Abstract**: The effects of sampling disturbance on the laboratory-derived mechanical properties of brittle rock were measured on cored samples of Lac du Bonnet granite taken from three different in situ stress domains at the Underground Research Laboratory of Atomic Energy of Canada Limited. A variety of independent measurements and scanning electron microscope observations demonstrate that stress-induced sampling disturbance increased with increasing in situ stresses. The degree of damage was reflected in laboratory measurements of acoustic velocity and elastic stiffness. Examination of the stress-induced microfracturing characteristics during uniaxial compression of the samples revealed that the degree of sampling disturbance had only minor effects on the stress levels at which new cracks were generated (i.e., the crack initiation stress threshold). Crack-coalescence and crack-damage thresholds, on the other hand, significantly decreased with increased sampling disturbance. The presence of numerous stress-relief cracks in the samples retrieved from the highest in situ stress domains was seen to weaken the rock by providing an increased number of planes of weakness for active cracks to propagate along. A 36% strength decrease was seen in samples retrieved from the highest in situ stress domain ($\sigma_1 - \sigma_3 \approx 40$ MPa) as compared with those taken from the lowest in situ stress domain ($\sigma_1 - \sigma_3 \approx 10$ MPa).

*Key words*: sample disturbance, brittle fracture, crack initiation, crack propagation, material properties, rock failure.

**Résumé** : Les effets du remaniement causé par le prélèvement sur les propriétés mécaniques déduites d'essais de laboratoire ont été mesurés sur des carottes de roche fragile en granite du Lac du Bonnet. Les carottages ont été effectués dans trois zones différentes de contraintes in situ, au Laboratoire de Recherche Souterrain de l'EACL au Canada. Une série de mesures indépendantes et d'observations au MEB démontrent que le remaniement de prélèvement dû aux contraintes augmente avec leur amplitude in situ. Le degré d'endommagement est reflété par les mesures, en laboratoire, de la vitesse de propagation acoustique et de la rigidité élastique. L'examen des caractéristiques de microfissuration induite par les contraintes pendant la compression axiale des éprouvettes a révélé que le degré de remaniement n'avait que des répercussions minimes sur les niveaux de contraintes auxquels de nouvelles fissures apparaissent (c'est-à-dire le seuil d'initiation des fissures, exprimé en termes de contraintes). D'un autre côté, les seuils de coalescence et de dommage causé par les fissures décroissent sensiblement lorsque le remaniement de prélèvement augmente. La présence de nombreuses fissures de relâchement de contraintes dans les carottes prélevées dans les zones à fortes contraintes in situ conduit à un affaiblissement de la roche par suite de l'existence d'un nombre accru de plans de faiblesse le long desquels les fissures actives se propagent. On a constaté un affaiblissement de 36% pour les échantillons prélevés dans la zone de fortes contraintes in situ ($\sigma_1 - \sigma_3 \approx 40$ MPa) par rapport à ceux qui proviennent de la zone à faible contraintes in situ ($\sigma_1 - \sigma_3 \approx 10$ MPa).

*Mots clés* : remaniement d'échantillon, rupture fragile, initialisation de fissure, propagation de fissures, propriétés des matériaux, rupture des roches.

[Traduit par la Rédaction]

## Introduction

The recovery and laboratory testing of drill core are fundamental steps in the geomechanical design of an underground excavation. Physical measurements obtained from core often provide the only direct means of quantifying the mechanical behaviour of the rock material. However, the process of drilling and recovering core may result in sample disturbance through stress-induced microfracturing altering the physical state of the rock (Guessous et al. 1984; Rathore et al. 1989; Martin and Stimpson 1994). This disturbance may be the result of mechanical abrasion and vibration during the drilling process, stress concentrations developed at the drill bit – rock contact, and (or) stress-relief cracking in cases where the samples are retrieved from high in situ stress regimes. Furthermore, a component of rock distur-

bance may be related to the in situ stress regime history and thus could vary from one point to another. In the most severe cases of sample disturbance, macrocracking and core discing can be observed (Obert and Stephenson 1965).

In general, the extent of sampling disturbance can be related to drilling depth, since in situ stresses generally increase with depth (Fig. 1). Martin and Stimpson (1994) note that it then becomes possible for samples with the same mineralogical composition but obtained from different depths, or in situ stress regimes, to have drastically different mechanical properties. This is an important point to consider when using laboratory test data, since the properties obtained for a given set of samples may not be truly representative of the undisturbed rock. For example, numerous studies have been performed on test samples of Lac du Bonnet granite as part of the Atomic Energy of Canada Limited (AECL) investigation into the permanent underground disposal of nuclear waste. The test material used in these studies varied in sampling location from surface quarries (e.g., Schmidtke and Lajtai 1985) to depths of 420 m depth (e.g., Martin and Chandler 1994). Jackson et al. (1989) and Martin and Stimpson (1994) reported the changes in acoustic velocity, Young's modulus, and uniaxial compressive strength for Lac du Bonnet granite with depth.

Recent work at the AECL Underground Research Laboratory (URL), however, has concentrated on using the crack initiation, $\sigma_{ci}$, and crack damage, $\sigma_{cd}$, stress thresholds to assess rock strength and progressive damage. Martin (1993) found that laboratory uniaxial compressive strength was not a unique material property but was partly dependent on loading conditions, whereas the crack-initiation and crack-damage stresses were more characteristic of the rock's in situ strength. The work presented in this paper, therefore, assesses the effects of sample disturbance on these stress-threshold characteristics in Lac du Bonnet granite.

Fig. 1. Sample disturbance as a function of depth, showing the change in material response in uniaxial compression from linear elastic to elasto-plastic with increasing sample damage (after Martin and Stimpson 1994). $\sigma$, stress; $\varepsilon$, strain.
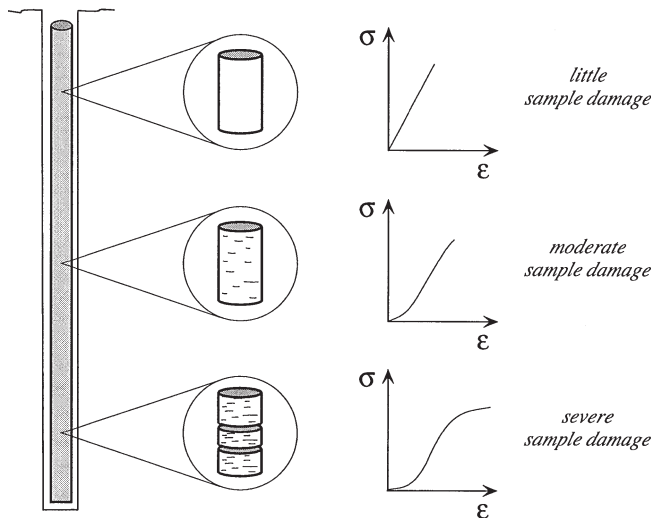


Fig. 2. Stress–strain diagram showing the stages of crack development (after Martin 1993). Note that only the axial ($\varepsilon_{axial}$) and lateral ($\varepsilon_{lateral}$) strains are measured; the volumetric and crack volume strains are calculated. $\sigma_{axial}$, axial stress; $\sigma_{ucs}$, peak stress.
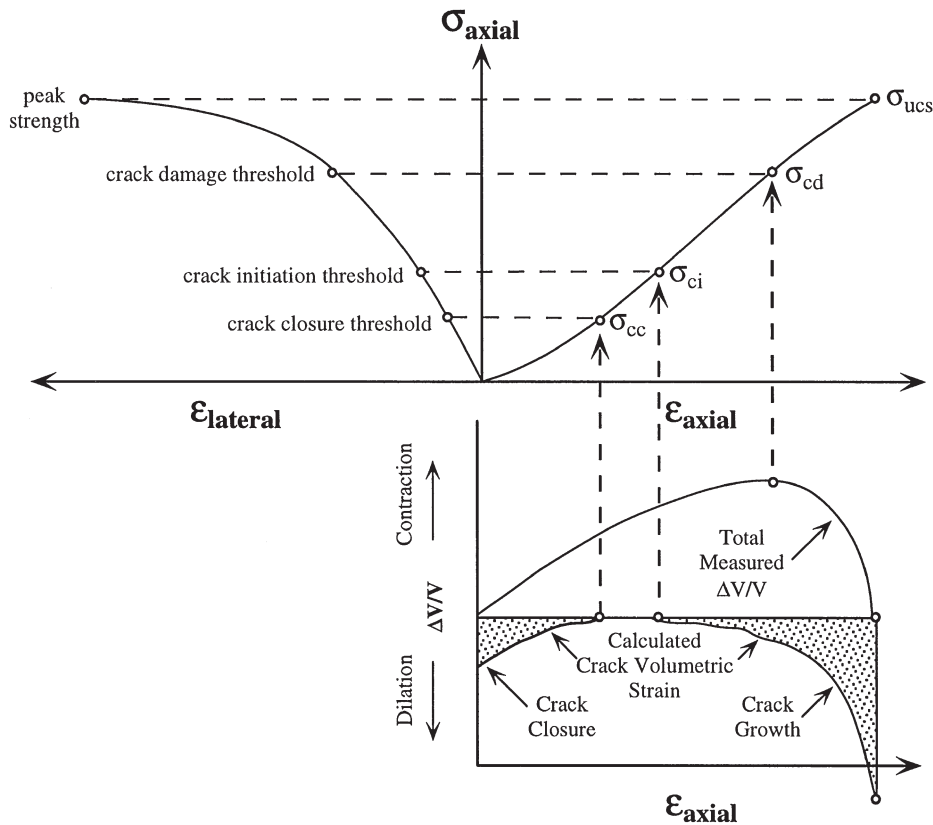
**Fig. 3.** Plot of the stress-dependent elastic impulse "energy" rate versus axial stress for a pink Lac du Bonnet granite from the 130 m level of the URL (after Eberhardt et al. 1999).
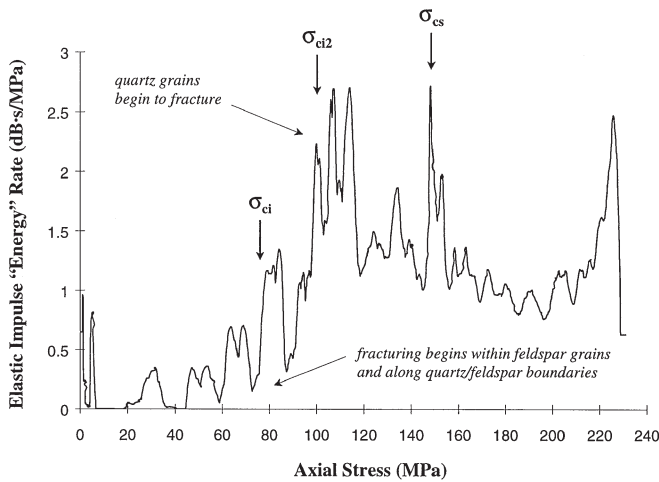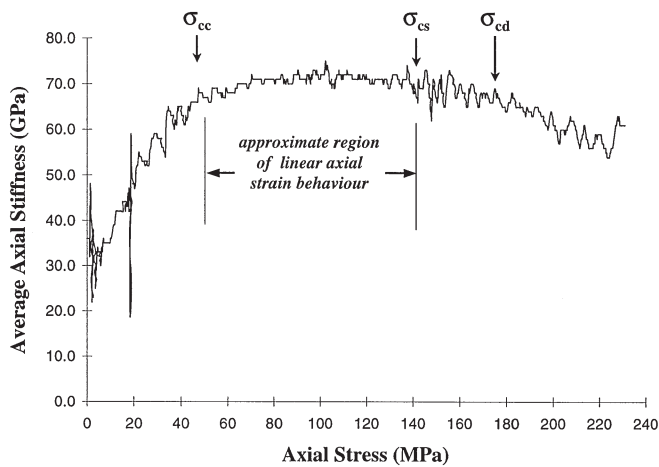


**Fig. 4.** Axial stiffness plot indicating a significant change in the axial strain rate following the crack-coalescence, $\sigma_{cs}$, threshold for a 130 m level URL pink granite (after Eberhardt et al. 1998).



**Fig. 5.** Volumetric stiffness versus axial stress plot showing the different stages of crack development for a Lac du Bonnet granite from the 130 m level of the URL (after Eberhardt et al. 1998).
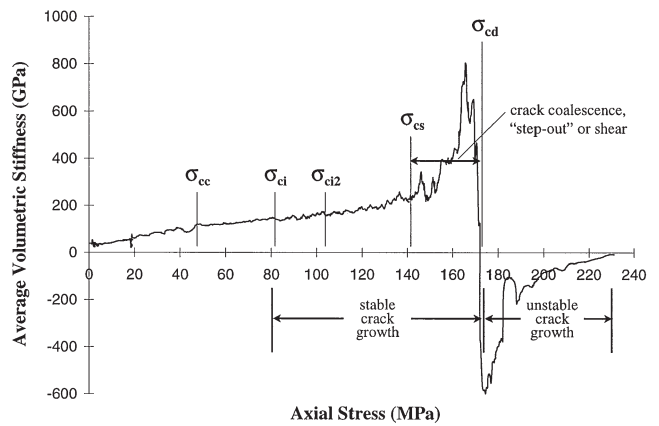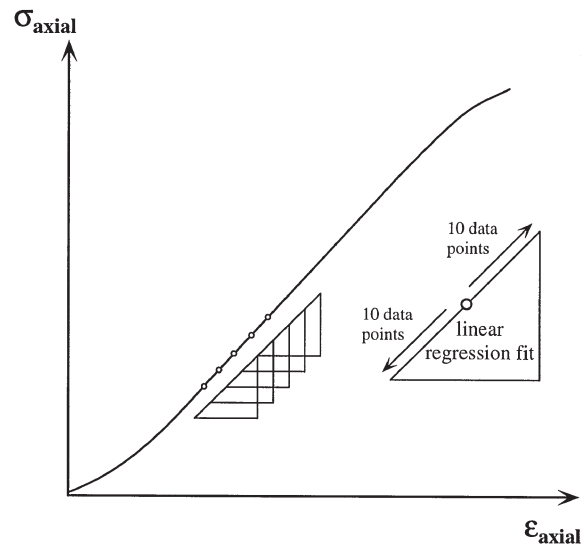


**Fig. 6.** Moving-point regression technique used for the generation of stress–strain stiffness plots, in this case one for an axial stress versus axial strain curve (the results for which are illustrated in Fig. 4).
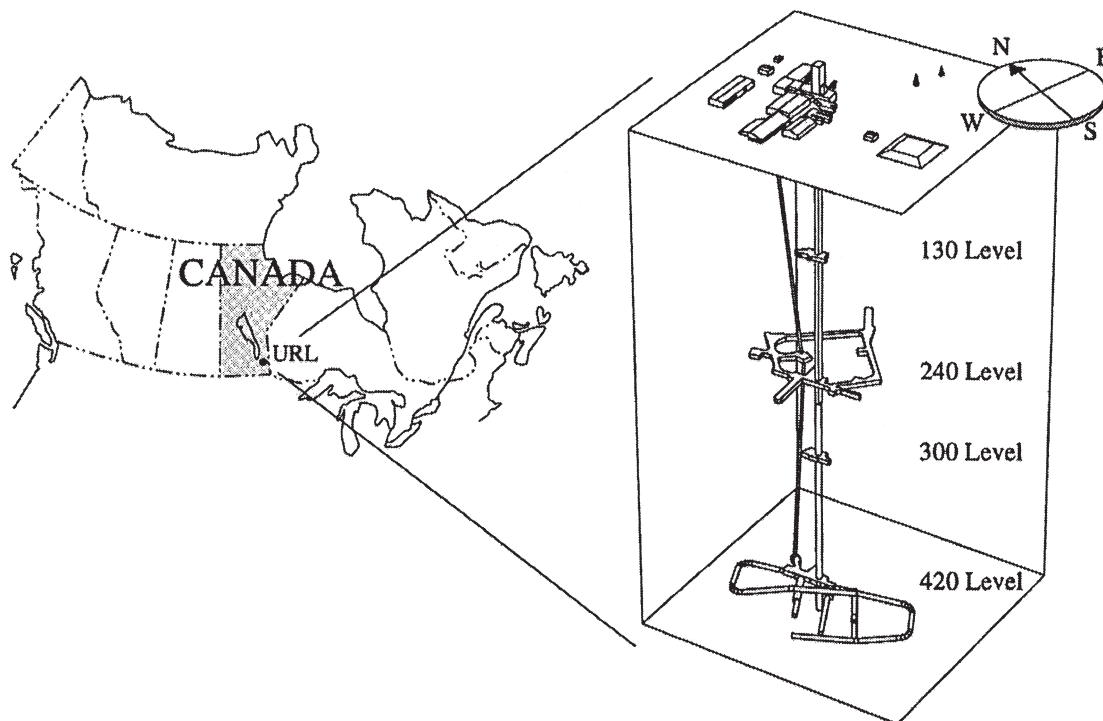


## Methodology

### Detection of stress-induced brittle microfracturing

The crack-initiation threshold, $\sigma_{ci}$, represents the stress level where microfracturing begins. Eberhardt et al. (1998) have demonstrated that this point can be determined through the combined use of electric resistance strain gauge and acoustic emission (AE) measurements. On a stress–strain curve, the threshold is defined as the point where the lateral- and volumetric-strain curves depart from linearity (Fig. 2). The initial propagation of these cracks is considered to be stable, as crack growth can be stopped by controlling the applied load. Unstable crack growth marks the point where the relationship between applied stress and crack length becomes less significant and other parameters, such as the crack growth velocity, take control of the propagation process (Bieniawski 1967). With reference to strain gauge measurements, the unstable crack propagation threshold has been associated with the point of reversal in the volumetric

strain curve, and is termed the crack damage stress threshold, $\sigma_{cd}$, by Martin (1993).

Eberhardt (1998) further showed that two intermediate crack thresholds between the crack-initiation and crack-damage thresholds also play key roles in the brittle-failure process of Lac du Bonnet granite. The first marks the initiation of cracking within the stronger quartz grains of the granite, as opposed to the initial cracking observed in the feldspar grains, and is termed the secondary crack-initiation threshold, $\sigma_{ci2}$. Figure 3 demonstrates how this point clearly stands out in a plot of the elastic impulse "energy" rate (it should be noted that this is not a true energy but is a relative measure derived from the AE event amplitude and duration). Eberhardt et al. (1999) have shown that the initiation of cracking, first in the feldspar grains and along weaker grain boundaries and second in the stronger quartz grains, can be

**Table 1.** Methodology used to establish the different thresholds of crack development.

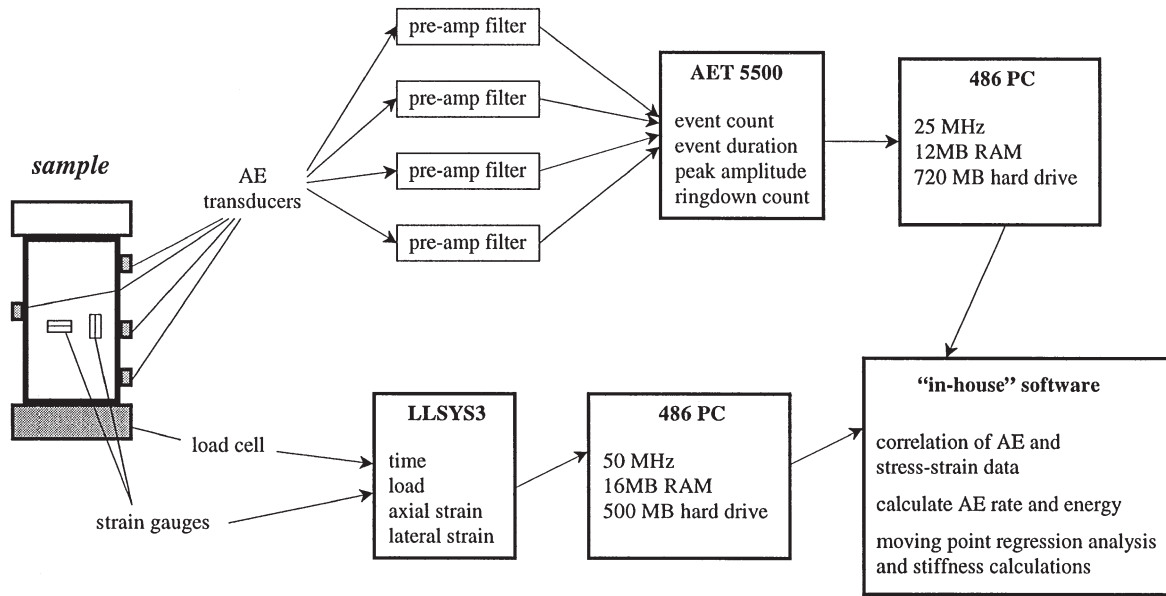| Crack threshold | Description |
| --- | --- |
| Crack closure ($\sigma_{cc}$) | The crack-closure threshold was established using the axial stiffness curve; the threshold value was determined as the point where the axial stiffness curve shifted from incrementally increasing values (i.e., nonlinear behaviour) to constant values (i.e., linear behaviour); linear axial strain behaviour was therefore used as an indicator that preferentially aligned cracks were closed |
| Crack initiation ($\sigma_{ci}$) | The crack-initiation threshold was based on several criteria; the primary criterion involved picking the approximate interval in which the AE event count first rose above the background level of detected events; the exact value within this interval could also be determined through the point in the AE event count rate and "energy" rate where values began to significantly increase; this point was checked against the first large break from linear behaviour in the volumetric stiffness plot |
| Secondary cracking ($\sigma_{ci2}$) | The secondary-cracking threshold was taken as the first significant increase in the AE event rate following crack initiation, which in turn coincided with the continuous detection of AE activity; furthermore, this point could be correlated with large increases in the event "energy" rate and notable breaks in the volumetric stiffness plot |
| Crack coalescence ($\sigma_{cs}$) | Crack coalescence was taken from the approximate interval in which the axial stiffness curve departed from linear behaviour (i.e., as an element of axial displacement was observed in the crack-propagation process); this point was checked against large irregularities in the volumetric stiffness curve; in addition, changes in the AE event rate and the different event properties would sometimes coincide with this point |
| Crack damage ($\sigma_{cd}$) | The crack-damage threshold was taken as the point in the volumetric stiffness curve where stiffness values changed from positive to negative, thereby marking the reversal of the volumetric strain curve |

**Fig. 7.** Location and layout of the Atomic Energy of Canada Limited Underground Research Laboratory (URL) (levels in metres).



**Table 2.** Approximate major ($\sigma_1$) and minor ($\sigma_3$) principal stress magnitudes for the three in situ stress domains of the URL (after Martin and Stimpson 1994).

| URL level (m) | $\sigma_1$ (MPa) | $\sigma_3$ (MPa) |
| --- | --- | --- |
| 130 | 10–20 | 5–10 |
| 240 | 25 | 12 |
| 420 | 55 | 14 |

differentiated using strain gauge, acoustic emission, and scanning election microscope (SEM) analysis.

The second of these intermediate thresholds is termed the crack-coalescence threshold, $\sigma_{cs}$, and marks the point where propagating cracks begin to interact and coalesce as they grow within the stress-concentration zones created by neighbouring cracks. This point is marked as a departure in linear axial strain behaviour, as nonlinearities are introduced through cracks coalescing at angles to the applied load and

**Fig. 8.** Schematic of strain gauge and acoustic emission instrumentation and data-collection systems.



through the collapse and rotation of grain material between coalescing crack tips. Figures 4 and 5 show the detection of this point through axial- and volumetric-stiffness plots, respectively (stiffness plots, described in detail by Eberhardt et al. 1998, use a moving point regression analysis of the stress–strain data set (Fig. 6) which acts to emphasize any inflections in the stress–strain curve). Each of the different stages of crack development and their respective stress thresholds were determined using a rigorous methodology based on strain gauge, acoustic emission, and AE event property measurements (Table 1). It should therefore be noted that the crack thresholds shown in the different plots (e.g., Figs. 3–5) were not solely determined through the plot depicting them but through a combination of the different analysis techniques utilized.

## Sample source and laboratory procedures

The Underground Research Laboratory has provided a means to investigate the effects of sampling disturbance by operating on two main levels (and two sub-levels) at different depths (Fig. 7). Core samples of Lac du Bonnet granite were obtained for this study from three different working levels at the URL located at depths of 130, 240, and 420 m. These levels represent three different in situ stress domains, each characterized by differing stress magnitudes and orientations. Martin (1993) and Read (1994) describe these regimes as varying from a low-stress domain (130 m level) associated with vertical or steeply inclined stress-relief jointing, to a transitional zone (240 m level) with moderate stresses, to a highly stressed region (420 m level) in unfractured rock. Values of the in situ stress magnitudes for these levels, as reported by Martin and Stimpson (1994), are provided in Table 2.

Testing was conducted at the University of Saskatchewan Rock Mechanics Laboratory on 61 mm diameter cylindrical samples prepared for testing according to American Society for Testing and Materials standards, with length to diameter ratios of approximately 2.25. Samples were instrumented

**Table 3.** Estimates of crack density from SEM observations of 130, 240, and 420 m level URL granite.

| URL level (m) | Minimum count (cracks/mm$^2$) | Maximum count (cracks/mm$^2$) |
|---|---|---|
| 130 | 0.005 | 0.01 |
| 130* | 1 | 5 |
| 240 | 0.01 | 0.05 |
| 420 | 10 | 20 |

*Samples loaded in uniaxial compression prior to analysis.

with six electric resistance strain gauges (three axial and three lateral at 60° intervals, 12.7 mm in length, with a 5% strain limit) and four 175 kHz resonant frequency, piezoelectric AE transducers. Uniaxial loading was applied at a constant rate of 0.25 MPa/s so that failure occurred between 5 and 10 min as recommended by the International Society for Rock Mechanics (Brown 1981). Applied loads and the resulting strains were recorded using an automatic data acquisition system, sampling at an average rate of two to three readings per second, thereby providing high data resolution. The AE monitoring system consisted of a bandpass filter with a frequency range of 125 kHz to 1 MHZ and a preamplifier with 40 dB total gain and a dynamic range of 85 dB. The AE data were recorded with an AET 5500 monitoring system using a threshold value of 0.1 V. A schematic of the system used is provided in Fig. 8.
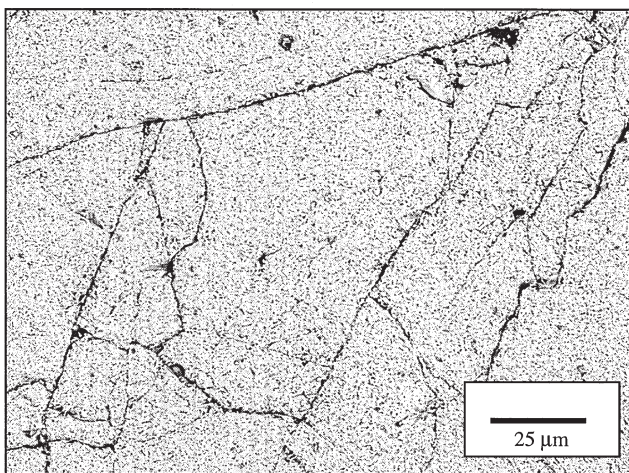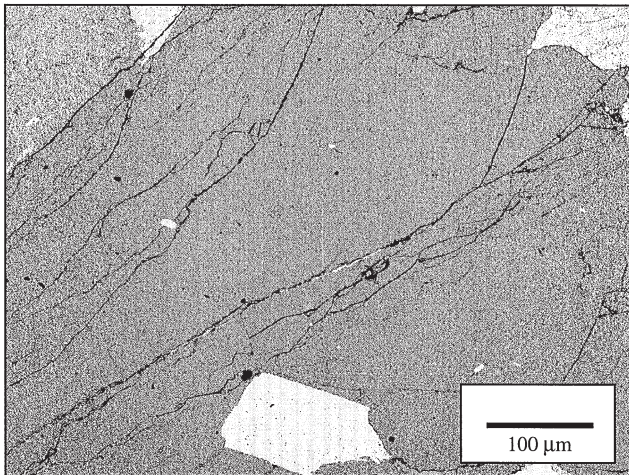
## SEM observations and acoustic velocity results

Prior to uniaxial compression testing, two samples of granite from each level (i.e., 130, 240, and 420 m) were selected for preparation of thin sections. SEM analysis of these sections showed that the density of observed microcracks increased significantly with depth. Whereas visible cracks were difficult to find in thin sections from the 130 and 240 m levels, numerous cracks were visible in sections from

the 420 m level. Estimates of crack density in these thin sections varied by three orders of magnitude (Table 3). Furthermore, thin sections of the 420 m level granite contained approximately five times more cracks than thin sections prepared from samples of 130 m level granite which had been previously loaded in uniaxial compression past the crack-damage threshold (Table 3). This was an unexpected result, since the maximum stresses experienced by the 130 m level granite samples during testing were approximately four times greater than those experienced by the 420 m level granite in situ.

The most notable difference between these granites was the high proportion of fractured quartz grains seen in the 420 m level sections (Fig. 9). Although intergranular frac-

**Fig. 9.** SEM image of two highly fractured quartz grains. Images are taken from sections prepared from core samples of the 420 m level Lac du Bonnet granite.



100 μm



25 μm

tures within quartz grains were observed in sections from the preloaded 130 m level samples, these fractures were often few in number and long, i.e., the few fractures induced by uniaxial compressive loading grew parallel to the direction of loading until they coalesced with one or two other neighbouring cracks. Conversely, the fractures observed in sections taken from the samples at the 420 m level have a shattered appearance. Although a preferred crack orientation can sometimes be seen in certain quartz grains, these cracks are typically intersected by a number of other cracks orientated at a variety of angles (Fig. 9). These fractures probably formed in response to high tensile stress gradients acting in the sample during stress relief (i.e., anelastic expansion) following drilling and core retrieval. It is also possible that a number of these cracks may have developed in situ as a result of high deviatoric stresses or stress rotations ahead of the drill hole.

The heavily fractured state of the 420 m level granite was reflected in acoustic velocity measurements which showed a significant reduction, approximately 30%, in both *P*- and *S*-wave velocities for the 420 m level samples relative to those from the 130 m level (Table 4). These results are similar to those presented by Martin and Stimpson (1994). Laboratory-measured *P*-wave velocities for the 130, 240, and 420 m level samples decrease by 18, 22, and 44%, respectively, when compared with the measured in situ value of 5900 m/s reported by Talebi and Young (1992). Similarly, laboratory *S*-wave values decrease by 12, 16, and 38% when compared with the measured in situ value of 3440 m/s (Fig. 10).
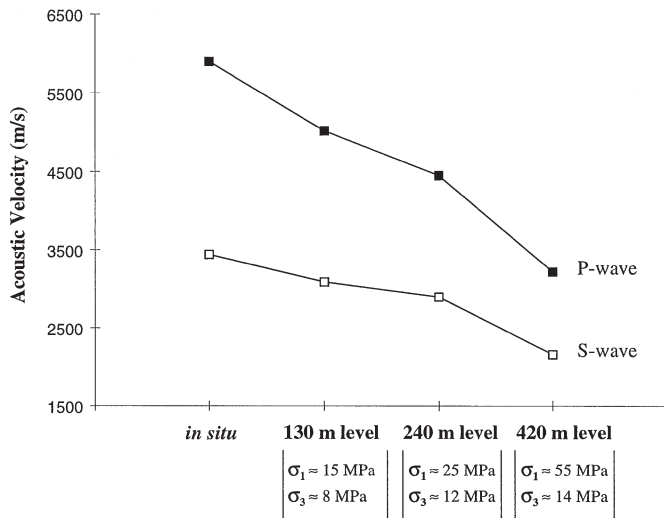
## Effect of increasing sample disturbance on deformation and fracture characteristics of Lac du Bonnet granite

Comparisons were first made between values of the secant and Young's moduli for granite samples from the 130, 240, and 420 m levels of the URL. It should be noted that the secant modulus, $E_S$, includes the initial nonlinearity in axial strain attributable to the closure of existing cracks, whereas the Young's modulus, $E$, is measured over the linear portion of the curve where it is assumed all cracks perpendicular to the applied load are closed (Fig. 11). The greater the degree of cracking induced during sampling, the more nonlinearity in the axial stress–strain curve upon initial loading and therefore the lower the secant modulus value. Test results show that the average secant modulus value for the 130 m level samples is only 8% lower than the average Young's modulus value, whereas the secant moduli for the 240 and 420 m level samples are 22 and 39% lower, respectively (Table 5). Secant modulus values for the 240 and 420 m level samples are 19 and 48% lower, respectively, than those

**Table 4.** Summary of density and acoustic velocity values for 130, 240, and 420 m level URL Lac du Bonnet granite samples (standard deviation in parentheses).

| Material parameter | 130 m level | 240 m level | 420 m level |
|---|---|---|---|
| Density ρ (g/cm$^2$) | 2.62 (±0.01) | 2.62 (±0.01) | 2.59 (±0.02) |
| *P*-wave velocity $V_P$ (m/s) | 4885 (±190) | 4445 (±295) | 3220 (±100) |
| *S*-wave velocity $V_S$ (m/s) | 3030 (±115) | 2905 (±85) | 2160 (±55) |
| $V_P/V_S$ ratio | 1.61 | 1.53 | 1.49 |

**Fig. 10.** *P*- and *S*-wave velocities for Lac du Bonnet granite samples from the 130, 240, and 420 m levels of the URL in comparison with in situ values.



**Fig. 11.** Method for calculating Young's modulus *E* and secant modulus $E_S$ from axial stress versus axial strain curves.
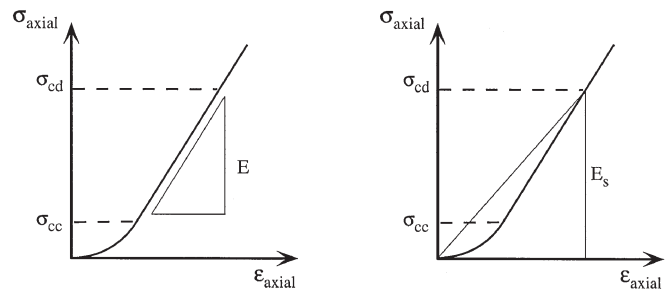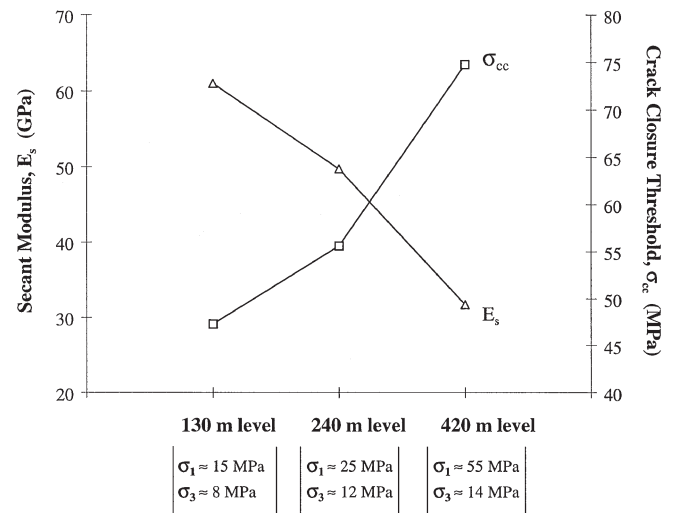


**Fig. 12.** Plots of secant modulus and crack-closure thresholds versus sampling depth for Lac du Bonnet granite samples from the 130, 240, and 420 m levels of the URL.



for the 130 m level. These differences are attributable to increasing sample disturbance, and therefore increasing crack densities, with depth. Furthermore, this induced form of damage was seen to effectively reduce the elastic stiffness of the rock matrix. The average Young's modulus for the 420 m level granite decreased by 22% when compared with the 130 m level values (Table 5). Poisson's ratio values were seen to increase by 23% when comparing 130 and 420 m level measurements. In comparison, Young's modulus and Poisson's ratio values for the 240 m level deviate by only 5% from 130 m level values. This emphasizes the relatively minor degree of sampling disturbance seen in the 240 m level samples compared to that incurred by the 420 m level samples.

The effect of sample disturbance was also clearly indicated through plots of the axial stiffness. As would be expected, increases in crack density due to higher degrees of stress-relief cracking resulted in larger crack-closure thresholds, $\sigma_{cc}$. This was previously reflected in decreasing secant modulus values (Fig. 12). Crack-closure thresholds for the 240 and 420 m level granites were 18 and 58% higher, respectively, than that for the 130 m level (Table 6). Plots of the axial stiffness versus axial stress for the different test sample groups (i.e., 130, 240, and 420 m levels) are also markedly different (Fig. 13). Damage was thus seen to not only increase the degree of nonlinear deformation exhibited during the initial stages of loading, but also induced a degree of "strain-softening" in the rock material.

The substantial effects sample disturbance had on the deformation and crack-closure parameters were not seen for the crack-initiation, $\sigma_{ci}$, and secondary-cracking, $\sigma_{ci2}$, thresholds. Table 6 shows only minor decreases with increasing sampling depth. Crack-initiation values for the 240 and 420 m level samples decreased by only 2 and 6%, respectively, when compared with those for the 130 m level. Secondary cracking values varied even less for the 240 and 420 m level samples, decreasing by 1 and 2% from 130 m level values. These results indicate that sampling disturbance has little effect on the initiation of new fractures. By

contrast, increased AE activity during crack closure was seen with increasing sampling disturbance (Fig. 14). These increases in AE activity are likely related to the closure and collapse of crack structures and bridging material between neighbouring crack tips (i.e., permanent strains), the number of which increases with sampling disturbance. In the case of the severely damaged 420 m level granite, the absence of any detected AE events prior to 40 MPa suggests that weaker crack structures had all but been destroyed or eliminated. Furthermore, the behaviour of these 420 m level samples appears to show greater plasticity during deformation. Given that the in situ stress difference (i.e., $\sigma_1 - \sigma_3$) on the 420 m level of the URL is also approximately 40 MPa (Table 3), the commencement of AE activity in the 420 m level granite may be a reflection of its previous stress history, otherwise known as the Kaiser effect (Holcomb 1993).

The test data show that sample disturbance does not significantly change the crack-initiation and secondary-cracking thresholds, therefore the reduction in compressive strength with sampling depth at the URL, reported by Jackson et al. (1989) and Martin and Stimpson (1994), must be associated with changes in how these cracks behave and interact once they begin to propagate. Analysis of the volumetric stiffness plots (i.e., moving point regression analysis (Fig. 6) performed on the axial stress versus volumetric strain curve) for the test samples reveals these changes and
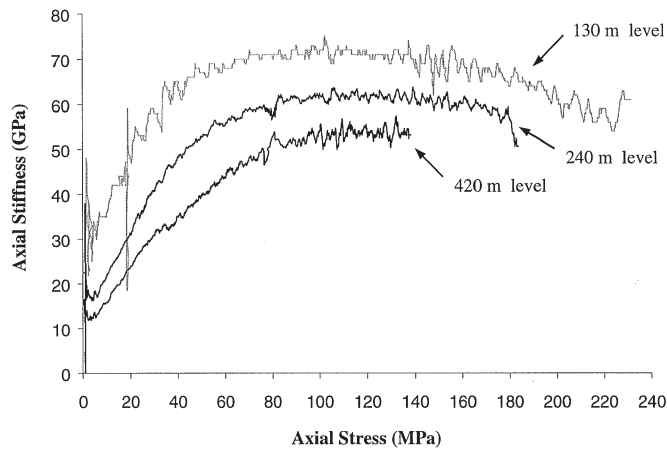
**Table 5.** Average elastic parameters for 130, 240, and 420 m level URL Lac du Bonnet granites (standard deviation in parentheses).

| Material parameter | 130 m level | 240 m level | 420 m level |
|---|---|---|---|
| No. of samples tested | 20 | 5 | 5 |
| Young's modulus $E$ (GPa) | 66.5 (±3.0) | 63.8 (±2.2) | 51.9 (±1.6) |
| Secant modulus $E_S$ (GPa) | 61.0 (±3.4) | 49.7 (±1.9) | 31.7 (±1.2) |
| Poisson's ratio $\nu$ | 0.31 (±0.04) | 0.33 (±0.04) | 0.38 (±0.04) |

**Table 6.** Average fracture parameters for 130, 240, and 420 m level URL Lac du Bonnet granites (standard deviation in parentheses).

| Strength parameter | 130 m level | 240 m level | 420 m level |
|---|---|---|---|
| No. of samples tested | 20 | 5 | 5 |
| Crack closure $\sigma_{cc}$ (MPa) | 47.3 (±2.7) | 55.6 (±1.5) | 74.8 (±1.0) |
| Crack initiation $\sigma_{ci}$ (MPa) | 81.5 (±3.7) | 79.6 (±2.3) | 76.4 (±3.7) |
| Secondary cracking $\sigma_{ci2}$ (MPa) | 103.9 (±5.0) | 102.8 (±4.3) | 102.0 (±2.5) |
| Crack coalescence $\sigma_{cs}$ (MPa) | 132.8 (±9.0) | 127.6 (±14.2) | 85.5 (±12.6) |
| Crack damage $\sigma_{cd}$ (MPa) | 156.0 (±13.2) | 147.4 (±9.1) | 100.4 (±12.2) |

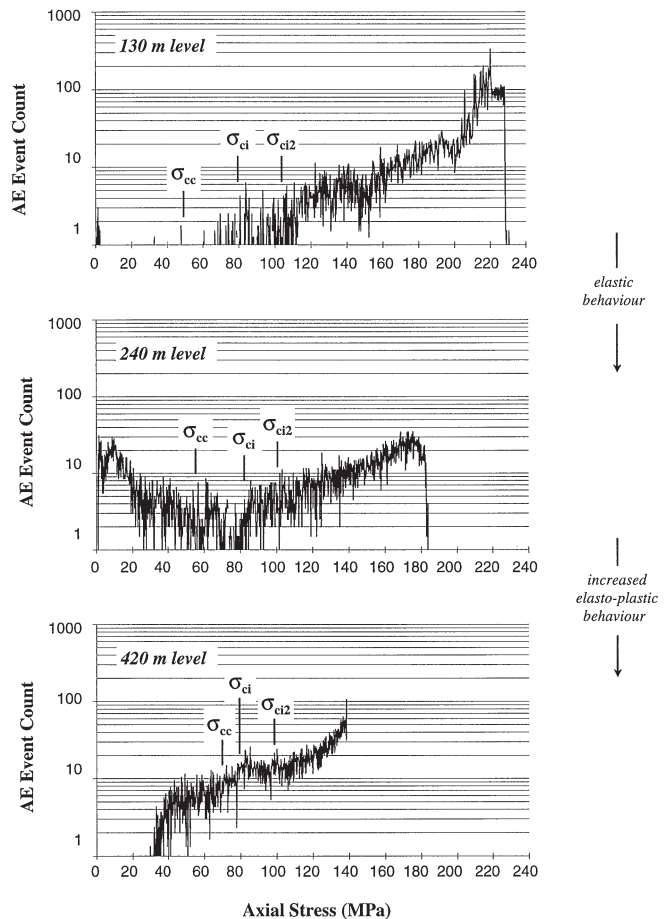**Fig. 13.** Plot of axial stiffness versus axial stress for Lac du Bonnet granite samples from the 130, 240, and 420 m levels of the URL.



**Fig. 14.** Logarithmic plots of AE event count versus axial stress for Lac du Bonnet granite samples from the 130 m (top), 240 m (middle), and 420 m (bottom) levels of the URL.



shows that the crack-coalescence, $\sigma_{cs}$, and crack-damage, $\sigma_{cd}$, thresholds decrease with increased sampling disturbance (Fig. 15). The small change in these values between the 130 and 240 m level granite reflects the small increase in in situ stress magnitudes between these levels (Table 6). Crack-coalescence and crack-damage thresholds for the 240 m level samples decrease by 4 and 6%, respectively, when compared with those for the 130 m level. The increase in in situ stress magnitudes on the 420 m level, however, is nearly two to three times that seen on the 130 and 240 m levels. Crack-coalescence and crack-damage values for these samples decrease substantially, 36 and 37% respectively, when compared with those for the 130 m level values.
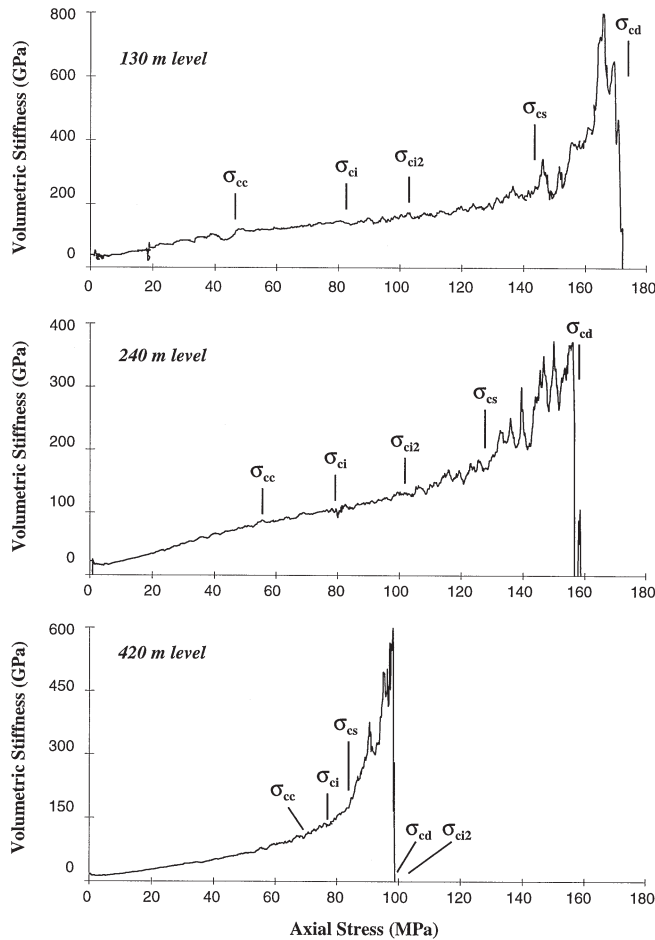
It follows then that stress-relief cracks may be viewed as planes of weakness, through which active cracks may propagate more easily. Cracks propagating in the 130 and 240 m level samples have stress-relief cracks, i.e., fewer planes of weakness, and therefore higher stresses are required to break through intact grains and along intact grain boundaries. Conversely, the large number of fractured grains and grain boundaries in the 420 m level samples (e.g., Fig. 9) provide a significant number of weak paths for cracks to propagate. Thus in a highly damaged sample, cracks may propagate more easily, resulting in their earlier coalescence and ulti-

**Fig. 15.** Plots of volumetric stiffness versus axial stress for Lac du Bonnet granite samples from the 130 m (top), 240 m (middle), and 420 m (bottom) levels of the URL.



**Fig. 16.** Plot of axial stiffness versus axial stress for a 420 m level Lac du Bonnet granite sample which never truly reaches a stage of linear elastic behaviour (i.e., highly nonlinear).



existing cracks induced from sample disturbance and new fractures initiated at the crack-initiation threshold were significant enough to lead to crack coalescence and volumetric strain reversal. The secondary-cracking threshold still appeared to be detectable in the AE data; however, the stress-induced fracturing of the intact quartz grains marked by this threshold likely only served to accelerate the failure of the samples. It is also possible that a significant proportion of quartz grains had already been fractured such that additional crack nucleation was not necessary for failure.

## Effects of grain size on the degree of sample disturbance

Additional testing was also performed on samples of finer grained granodiorite taken from the 240 and 420 m levels of the URL so that the effects of grain size on the degree of sampling disturbance could be investigated. The granodiorite in the Lac du Bonnet batholith is interspersed with the granites, primarily below 200 m, in the form of dykes. The granodiorite is similar in mineralogy to the granite but has an average grain size of 1 mm, whereas the average grain size of the granite is approximately 3 mm. It should also be noted that the grains in the granodiorite are equidimensional, whereas those in the granite are not. SEM observations suggest that the density of microcracks attributable to sample disturbance in the granodiorite from the 420 m level was significantly lower than that seen in the 420 m level granite ($0.25$ cracks/mm$^2$ as opposed to $10$ cracks/mm$^2$). Cracks in the granodiorite thin sections were predominantly found along grain boundaries and within feldspar grains. Fractured or shattered quartz grains, which were frequently observed in thin sections taken from the 420 m level granite, were not apparent in the 420 m level granodiorite sections.

SEM analysis of the 420 m level granodiorite samples also revealed that the crack density, although not as high as those in the 420 m level granites, was still considerably higher than those seen in the 130 and 240 m level granite samples. The damaged state of the granodiorite samples was also reflected in density and acoustic velocity measurements conducted prior to uniaxial compression testing. The 420 m level granodiorite had slightly higher (5%) acoustic velocities than the 420 m level grey granite but significantly lower
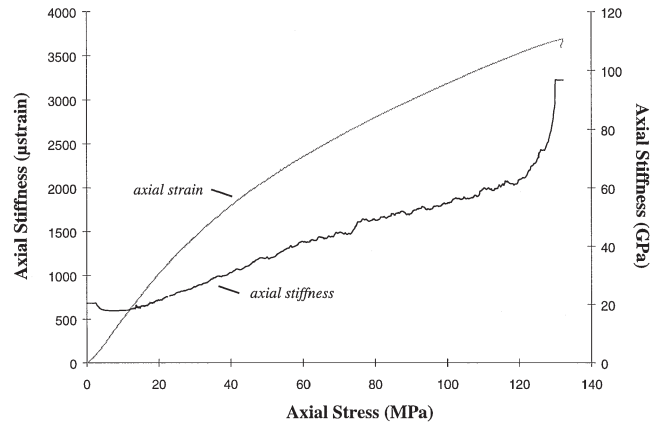
mately the failure of the sample at a lower compressive stress.

For highly damaged samples several of the stages of crack development either overlap with one another or proceed in a different order than that for less damaged rock. For example, Table 6 shows that the crack-closure threshold, $\sigma_{cc}$, for the 420 m level samples was approximately the same magnitude as the crack-initiation threshold, $\sigma_{ci}$. This "overlap" may reflect changes in the axial and lateral strain rates which are occurring due to both the initiation of new cracks and deformations in the form of grain boundary – crack sliding. If new cracks are forming while existing ones have yet to close, the axial stiffness may never reach linear elastic behaviour but continue to change in a nonlinear fashion throughout loading (Fig. 16). In such cases, crack closure as it is presently defined is never truly reached and detection of the crack-initiation and secondary-cracking thresholds are only discernable in the acoustic emission data.

It was also observed that the secondary-cracking threshold for the 420 m level granite was preceded by the crack-coalescence and crack-damage thresholds (Fig. 15). In both the 130 and 240 m level granites, secondary cracking preceded both crack coalescence and crack damage. This difference would suggest that the propagation and interaction of

**Table 7.** Average index and deformation parameters for samples of 420 m level Lac du Bonnet granite and granodiorite and 240 m level Lac du Bonnet granodiorite from the URL (standard deviation in parentheses).

| Material parameter | 420 m level grey granite | 420 m level granodiorite | 240 m level granodiorite |
|---|---|---|---|
| No. of samples tested | 5 | 5 | 5 |
| Density $\rho$ (g/cm$^3$) | 2.59 ($\pm$0.02) | 2.63 ($\pm$0.01) | 2.66 ($\pm$0.00) |
| $P$-wave velocity $V_P$ (m/s) | 3220 ($\pm$100) | 3335 ($\pm$105) | 5240 ($\pm$70) |
| $S$-wave velocity $V_S$ (m/s) | 2160 ($\pm$55) | 2310 ($\pm$35) | 3245 ($\pm$60) |
| $V_P/V_S$ ratio | 1.49 | 1.44 | 1.61 |
| Young's modulus $E$ (GPa) | 51.9 ($\pm$1.6) | 57.7 ($\pm$0.9) | 63.8 ($\pm$2.2) |
| Secant modulus $E_S$ (GPa) | 31.7 ($\pm$1.2) | 40.2 ($\pm$1.5) | 49.7 ($\pm$1.9) |
| Poisson's ratio $\nu$ | 0.38 ($\pm$0.04) | 0.34 ($\pm$0.01) | 0.33 ($\pm$0.04) |

**Table 8.** Average fracture parameters for 420 m level Lac du Bonnet granite and granodiorite and 240 m level Lac du Bonnet granodiorite from the URL (standard deviation in parentheses).

| Strength parameter | 420 m level grey granite | 420 m level granodiorite | 240 m level granodiorite |
|---|---|---|---|
| No. of samples tested | 5 | 5 | 5 |
| Crack closure $\sigma_{cc}$ (MPa) | 74.8 ($\pm$1.0) | 70.4 ($\pm$7.9) | 45.6 ($\pm$3.4) |
| Crack initiation $\sigma_{ci}$ (MPa) | 76.4 ($\pm$3.7) | 79.6 ($\pm$4.5) | 79.6 ($\pm$2.7) |
| Secondary cracking $\sigma_{ci2}$ (MPa) | 102.0 ($\pm$2.5) | 100.8 ($\pm$2.7) | 102.8 ($\pm$4.5) |
| Crack coalescence $\sigma_{cs}$ (MPa) | 85.5 ($\pm$12.6) | 122.0 ($\pm$11.5) | 164.7 ($\pm$9.0) |
| Crack damage $\sigma_{cd}$ (MPa) | 100.4 ($\pm$12.2) | 152.4 ($\pm$3.4) | 194.0 ($\pm$2.8) |
| Peak strength $\sigma_{ucs}$ (MPa) | 157.1 ($\pm$17.7) | 209.0 ($\pm$3.7) | 221.5 ($\pm$21.3) |

(34%) values than the 240 m level granodiorites. Table 7 shows that the 420 m level granodiorite, as compared with the 420 m level granite, has a higher density, $P$- and $S$-wave velocities, and Young's and secant moduli. Much larger disparities exist when comparisons are made between 420 and 240 m level granodiorite values. It can therefore be concluded that granodiorite samples from the 420 m level have been subjected to a higher degree of microfracturing prior to testing than those from the 240 m level granodiorite.

Crack thresholds for the 420 m level granodiorite, however, follow the same patterns of crack development as those seen in the lesser damaged samples (e.g., 240 m level granodiorite). Crack-closure values are similar to those for the 420 m level granites, but values for the crack-initiation and secondary-cracking thresholds did not significantly vary (Table 8), showing that their values are more closely related to the strengths of the individual feldspar and quartz minerals than grain size. Grain size did, however, have a significant effect on the crack-coalescence and crack-damage thresholds of the 420 m level samples. Crack-coalescence and crack-damage values for the finer grained 420 m level granodiorite were 30 and 34% higher, respectively, than those for the coarser grained 420 m level granite (Table 8). Furthermore, the number of detected AE events for the granodiorite was lower than that for the granite (Fig. 17). The effects of sampling disturbance on the granodiorite were also evident in that the crack-coalescence, $\sigma_{cs}$, and crack-damage, $\sigma_{cd}$, values for the 240 and 420 m levels differed by 26 and 21%, respectively (Fig. 18). Overall, the fine-grained, equidimensional nature of the 420 m level granodiorite appeared to limit the extent of crack propagation, thereby resulting in higher compressive strengths than

for the 420 m level granite, yet sampling disturbance did reduce its strength relative to the 240 m level granodiorite (Table 8).
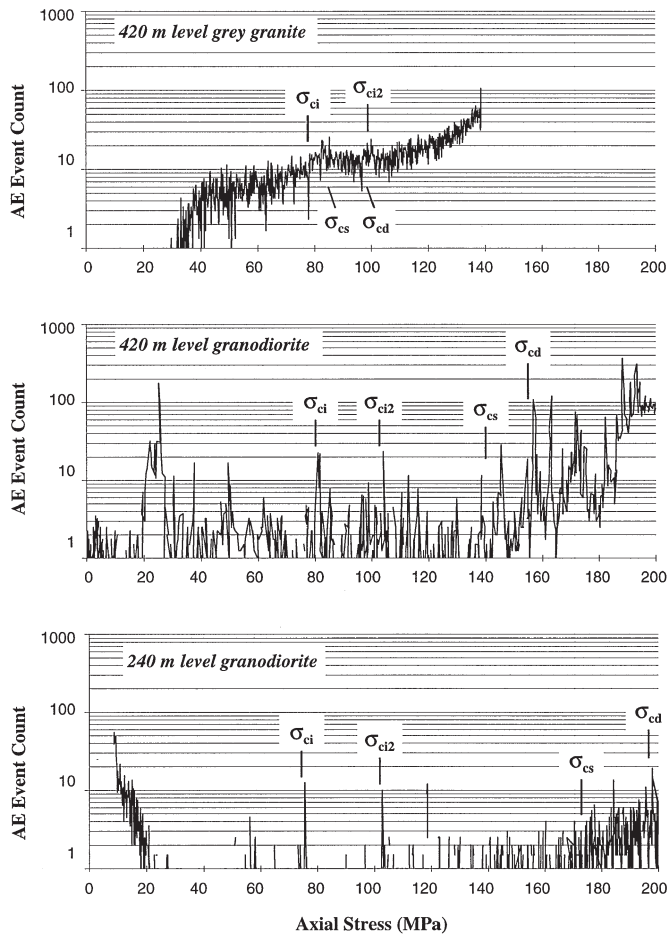
## Conclusions

In cases where laboratory test samples of brittle rock have undergone significant sampling disturbance, the mechanical properties of the samples will be quite different from those of their in situ state. Sampling-disturbance effects measured on granite and granodiorite samples loaded in uniaxial compression and taken from three different in situ stress regimes of the URL (i.e., 130, 240, and 420 m levels corresponding to $\sigma_1 - \sigma_3$ values of 7.5, 13, and 41 MPa, respectively) led to the following observations:

(1) Acoustic velocities and material stiffness values decreased with depth of sampling. These reductions are attributed to increased stress-induced sampling disturbance. Substantial damage was found in samples obtained from the 420 m level. These observations were confirmed through SEM images which showed that crack densities in the samples increased markedly with sampling depth. $P$- and $S$-wave velocities and Young's and secant moduli also decreased with increased sampling disturbance.

(2) Sampling disturbance had only minor effects on the initiation of new fractures. As the applied stress approached the crack-initiation and secondary-cracking thresholds, new fracturing began within those grains and along those grain boundaries which had not been damaged during sampling disturbance. Increasing AE counts with increased sample disturbance prior to these points suggested that higher crack

**Fig. 17.** Logarithmic plots of AE event count versus axial stress for URL samples of 420 m level Lac du Bonnet granite (top), 420 m level Lac du Bonnet granodiorite (middle), and 240 m level Lac du Bonnet granodiorite (bottom).



**Fig. 18.** Plots of volumetric stiffness versus axial stress for URL samples of 420 m level Lac du Bonnet granite (top), 420 m level Lac du Bonnet granodiorite (middle), and 240 m level Lac du Bonnet granodiorite (bottom).



densities resulted in more AE activity related to grain boundary movements and the collapse of crack structures.
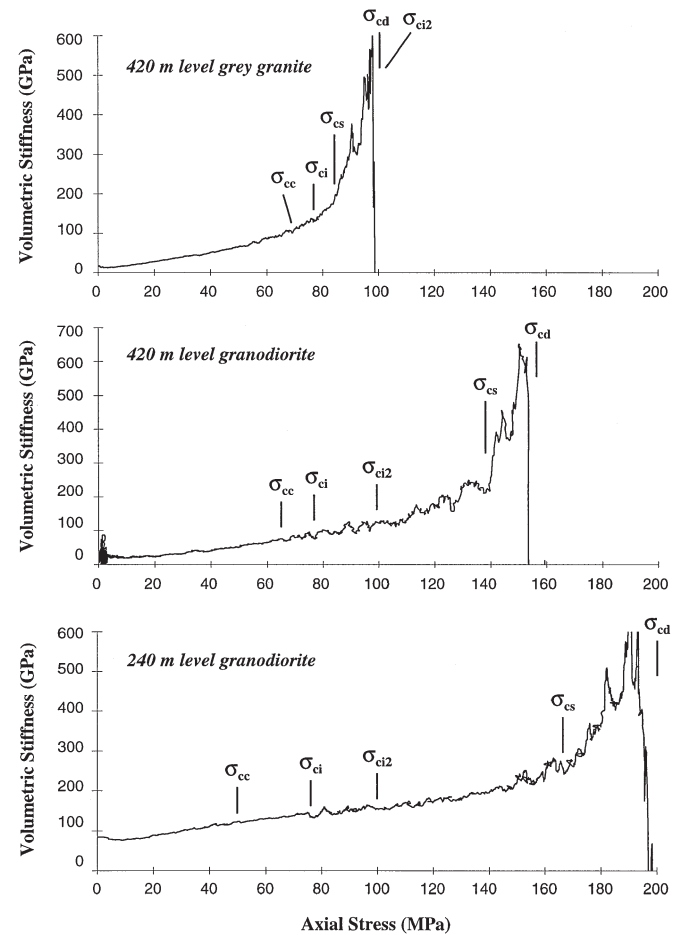
(3) Crack-coalescence and crack-damage thresholds decreased significantly with increased sampling disturbance. The presence of numerous stress-relief cracks in the 420 m level samples weakened the rock by providing an increased number of planes of weakness for cracks to propagate along. It is suggested that in the highly damaged samples, cracks may propagate more easily, resulting in their earlier coalescence and ultimately the failure of the sample at lower compressive stress.

(4) The extent of damage in the 420 m level granite was not observed in samples of the 420 m level granodiorite. The equidimensional, fine-grained nature of the granodiorite appears to limit the extent of crack propagation and interaction, thereby resulting in higher compressive strengths than the granite. However, the presence of sampling disturbance did reduce the strength of the 420 m level granodiorite relative to that of the 240 m level granodiorite.

## Acknowledgments

## References

Bieniawski, Z.T. 1967. Mechanism of brittle rock fracture: Part I. Theory of the fracture process. International Journal of Rock Mechanics and Mining Sciences & Geomechanics Abstracts, **4**(4): 395–406.

Brown, E.T. 1981. Rock characterization testing and monitoring: ISRM suggested methods. Pergamon Press Ltd., Oxford.

Eberhardt, E. 1998. Brittle rock fracture and progressive damage in uniaxial compression. Ph.D. thesis, Department of Geological Sciences, University of Saskatchewan, Saskatoon.

Eberhardt, E., Stead, D., Stimpson, B., and Read, R.S. 1998. Identifying crack initiation and propagation thresholds in brittle rock. Canadian Geotechnical Journal, **35**(2): 222–233.

Eberhardt, E., Stead, D., and Stimpson, B. 1999. The influence of mineralogy and grain boundaries on the initiation of microfracturing in granite. *In* Proceedings of the 8th International Congress on Rock Mechanics, Paris, August 25–28, 1999. In press.

Guessous, Z., Ladanyi, B., and Gill, D.E. 1984. Effect of sampling disturbance on laboratory determined properties of rock salt. *In* The Mechanical Behaviour of Salt, Proceedings of the 2nd Conference, Hanover. *Edited by* H.R. Hardy Jr. and M. Langer. Trans Tech Publications, Clausthal-Zellerfeld, Germany, pp. 137–158.

Holcomb, D.J. 1993. General theory of the Kaiser effect. International Journal of Rock Mechanics and Mining Sciences & Geomechanics Abstracts, **30**(7): 929–935.

Jackson, R., Lau, J.S.O., and Annor, A. 1989. Mechanical, thermo-mechanical & joint properties of rock samples from the site of AECL's Underground Research Laboratory, Lac du Bonnet, Manitoba. *In* Materials: From Theory to Practice, Proceedings of the 42nd Canadian Geotechnical Conference, Winnipeg. Canadian Geotechnical Society, Toronto, pp. 41–49.

Martin, C.D. 1993. Strength of massive Lac du Bonnet Granite around underground openings. Ph.D. thesis, Department of Civil and Geological Engineering, University of Manitoba, Winnipeg.

Martin, C.D., and Chandler, N.A. 1994. The progressive fracture of Lac du Bonnet granite. International Journal of Rock Mechanics and Mining Sciences & Geomechanics Abstracts, **31**(6): 643–659.

Martin, C.D., and Stimpson, B. 1994. The effect of sample disturbance on laboratory properties of Lac du Bonnet granite. Canadian Geotechnical Journal, **31**(5): 692–702.

Obert, L., and Stephenson, D.E. 1965. Stress conditions under which core discing occurs. Society of Mining Engineers of AIME Transactions, **232**(3): 227–235.

Rathore, J.S., Holt, R.M., and Fjaer, E. 1989. Effects of stress history on petrophysical properties of granular rocks. *In* Rock Mechanics as a Guide for Efficient Utilization of Natural Resources, Proceedings of the 30th U.S. Symposium on Rock Mechanics, Morgantown. *Edited by* A.W. Khair. A.A. Balkema, Rotterdam, The Netherlands, pp. 765–772.

Read, R.S. 1994. Interpreting excavation-induced displacements around a tunnel in highly stressed granite. Ph.D. thesis, Department of Civil and Geological Engineering, University of Manitoba, Winnipeg.

Schmidtke, R.H., and Lajtai, E.Z. 1985. The long-term strength of Lac du Bonnet granite. International Journal of Rock Mechanics and Mining Sciences & Geomechanics Abstracts, **22**(6): 461–465.

Talebi, S., and Young, R.P. 1992. Microseismic monitoring in highly stressed granite: relation between shaft-wall cracking and in situ stress. International Journal of Rock Mechanics and Mining Sciences & Geomechanics Abstracts, **29**(1): 25–34.